Tracing the origin of radio emission in galaxies with superMIGHTEE

Sthabile Kolwa[1], Russ Taylor[2,3], Sushant Dutta[2], Dharam V. Lal[4], Lennart Heino[2] and Mattia Vaccari[2,3]

[1]Department of Mathematical Sciences, University of South Africa, Cnr Christian de Wet Rd and Pioneer Avenue, Florida Park, 1709, Roodepoort, South Africa
[2]Inter-University Institute for Data Intensive Astronomy, Department of Astronomy, University of Cape Town, Private Bag X3,Rondebosch, 7701, Cape Town, South Africa
[3]Inter-University Institute for Data Intensive Astronomy, Department of Physics and Astronomy, University of the Western Cape,Robert Sobukwe Road, Bellville, 7535, Cape Town, South Africa
[4]National Centre for Radio Astrophysics - Tata Institute of Fundamental Research Post Box 3, Ganeshkhind P.O., Pune 411007, India

E-mail: kolwasn@unisa.ac.za

Abstract. Detailed modelling of radio spectral energy distributions. With the recent availability of catalogues of radio sources detected with interferometers such as MeerKAT (Meer Karoo Array Telescope) and the upgraded Giant Metrewave Radio Telescope (uGMRT) have sufficient observational sensitivity to detect the faintest radio emission in galaxies. For this, we make use of the superMIGHTEE survey which combines data from the MIGHTEE (MeerKAT International GigaHertz Extragalactic Exploration) survey and the uGMRT. At this faint flux end, it is generally unclear which specific mechanisms produce radio emission. In this foundational study, we begin to tackle this quandary by obtaining constraints on spectral curvature using four-band radio detections spanning observed frequencies of 100 MHz - 2 GHz for radio-loud AGN. Considering the Eddington and Malmquist biases which skew our results at low and high radio fluxes, respectively, we find a dominance of steep spectrum sources among the radio-loud active galactic nuclei (AGN) population indicative of synchrotron processes originating from the jets and lobes. For non radio-loud AGN (assumed to be normal star-forming galaxies and radio-faint AGN), we see a predominance of flat spectra associated with thermal processes occurring in HII regions.

1 Introduction

Wide-field extragalactic radio continuum surveys are an essential tool in galaxy evolution. Observing over frequencies of approximately 10 MHz - 10 GHz. With these surveys, it is possible to probe both nuclear activity and star-formation in galaxies through cosmic time [1]. HII regions produce synchrotron radiation due to the acceleration of cosmic ray electrons within the plasma surrounding supernova remnants as well as free-free emission [2]. At the nuclei of active galaxies, jets produced through accretion of gas onto the black-hole also accelerate relativistic electrons forming non-thermal synchrotron emission contributing to the radio continuum observed [3, 4]. With sufficient detection sensitivity, radio continuum surveys can detect wide samples of star-forming galaxies, radio-quiet quasars and low-luminosity radio galaxies [5]. An additional benefit is a contraint of star-formation rates and histories that are which do not require dust attenuation corrections due to the centimetre wavelengths of radio radiation [6].

With sensitive radio survey detections of nuclear activity and star-formation in galaxies, two distinct populations of sources emerge: active galactic nuclei (AGN) and star-forming galaxies (SFGs), where radio emission originates from the nucleus and star-forming regions, respectively [7]. The faint radio source population, in particular emerges at 1.4 GHz radio flux densities of approximately ≤ 1.0 mJy. The jet- and radiative-mode populations of radio galaxies also known as radio-loud active galactic nuclei are the most powerful radio sources and dominate at flux densities of > 1 mJy. Within the sub-mJy population, however, star-forming galaxies and young or restarted AGN host galaxies are the dominant groups of sources [8, 9, 10]. The radio-loud AGN population has been well studied in terms of both the AGN and host galaxy properties up to $z \sim 1.0$ [11]. The emerging faint source population at low redshifts, however, provide a new frontier for investigating the mechanisms powering radio emission in radio-quiet/faint AGN and star-forming galaxies on a statistical scale.

We can make use of radio spectral energy distributions (SEDs) to trace the origin of radio emission in galaxies [12]. When sufficient multi-frequency observations are available, we can fit emission models to the radio spectra to determine the underlying physics producing the radiation seen. The models are based on well-studied radio spectra of objects in the nearby Universe. It is known, for instance, that at rest-frame frequencies of $1.0 \leq \nu_0 \leq 10$ GHz, spectral steepening is attributed to energy losses in cosmic ray electrons due to Inverse-Compton scattering as well as synchrotron radiation in optically thin plasma regions [13]. At lower rest-frame frequencies of $\nu_0 \leq 1$ GHz, steepening of radio spectra result from synchrotron self-Compton scattering in the optically thick plasma and also free-free absorption along the line-of-sight. Both these processes have been constrained in the radio spectra of nearby SFGs and the Galactic Centre [].

In situations where a sample of sources has incomplete data, however, and only a few radio frequency bands have significant ($> 5\sigma$) detections, it may not be possible to fit models to an SED. Rather, we will need to rely on the spectral index, α from the power law relation $S_\nu \propto \nu^\alpha$ to measure the gradient of a radio SED on a logarithmic scale. A measure of α can provide a first glimpse into the origin of the emission at an observed frequency which we deproject with the redshift information available.

Focussing on the poorly understood faint radio source population, we aim to determine what primarily powers the radio emission in radio-quiet or non-jetted AGN population - star-formation or the faint AGN? Now that we are able to detect a significant number of sources in the sub-mJy flux density range, we wish to investigate whether spectra are predominantly flat across the population and if so, whether this is due to thermal or non-thermal radiation. With recent observations from the MIGHTEE (MeerKAT International GigaHertz Tiered Extragalactic Exploration) Survey [1] and surveys conducted with the upgraded Giant Metrewave Radio Telescope (uGMRT), we can detect the faint radio source population down to an rms (root mean square) noise threshold of approximately 2 μJy in flux. The comparable flux limits between MIGHTEE and uGMRT make the samples complete meaning we are able to properly constrain radio spectral indices across three bands for thousands of sources. With this sample, we can infer the radiative processes responsible for the radio emission for the non-jetted AGN and SFGs observed.

2 The superMIGHTEE Survey of XMM-LSS

superMIGHTEE refers to combination of survey data from the MIGHTEE project and uGMRT observations to produce deep radio continuum images at μ Jy sensitivity over a frequency range of 200 MHz to 2.5 GHz. The surveys are resolution-matched at $\sim 5''$. In this work, we make use of the MIGHTEE DR1 survey of the *XMM-Newton* Large Scale Structure Survey (XMM-LSS) field [14]. The XMM-LSS image mosaic comprises 45 MeerKAT pointings with a total integration time of 297.9 h. The image is taken in the L-band at a central frequency of 1.28 GHz. During calibration and imaging, a robust weighting parameter of -1.2 is applied to produce an image with a restoring beam of size $5'' \times 5''$ and a thermal noise level of 3.4 μJy/beam. The uGMRT DR1 Survey of XMM-LSS consists of two observing frequencies: band-3 centred at 390 MHz and band-4 at 690 MHz (Lal et al. 2025, in press). The survey coverage of superMIGHTEE are shown against that of LOFAR 144 MHz in Figure 1(a).

2.1 Ancillary Data and Redshifts

Additional multiwavelength information on the radio sources in XMM-LSS are available from legacy surveys. We use an optical/near-infrared (NIR) catalogue comprising $YJHK_s$ photometry from the VISTA telescope's VIDEO (VISTA Deep Extragalactic Observations) Survey [15]. Additionally, we have optical photometry from the GRIZy filters of the HyperSuprimeCam(HSC) *Subaru* Strategic Program (SSP) [16]. The observed photometric data are fit to emission templates using `LePHARE` [17]. Additionally, photometric estimations are obtained using the GPz machine learning procedure [18]. A consensus redshift is determined from both methods using a hierarchical Bayesian method described in [19].

2.2 *Radio and optical/NIR cross-matching*

We obtain radio catalogues of sources from the images by running the Python Blob and Detection Source Finder (PyBDSF) [20]. With these we can perform an sky cross-match of radio sources to find their optical counterparts. In this, we find the nearest optical/NIR source in projection to a radio source within $1.2''$. The number of radio sources in uGMRT band-3, band-4, and MIGHTEE L-band are 10,931, 16,284 and 72,187, respectively. After performing the radio-optical cross-matching we find 7,849, 14,129, and 31,763 radio sources with optical counterparts giving a 72%, 87%, and 44% completeness, respectively. The combined radio and optical/NIR catalogue provide redshifts for sources with optical counterparts. With this information, we can calculate radio luminosity at a reference frequencies of ν_0 using the relation,

$$L_{\nu,0} = 4\pi(\nu_0/\nu)^{\alpha} d_L^2 (1+z)^{-\gamma} S_\nu, \tag{1}$$

where ν is the observing frequency, d_L is the luminosity distance, and $\gamma = \alpha + 1$. We adopt a canonical spectral index of $\alpha = -0.7$.

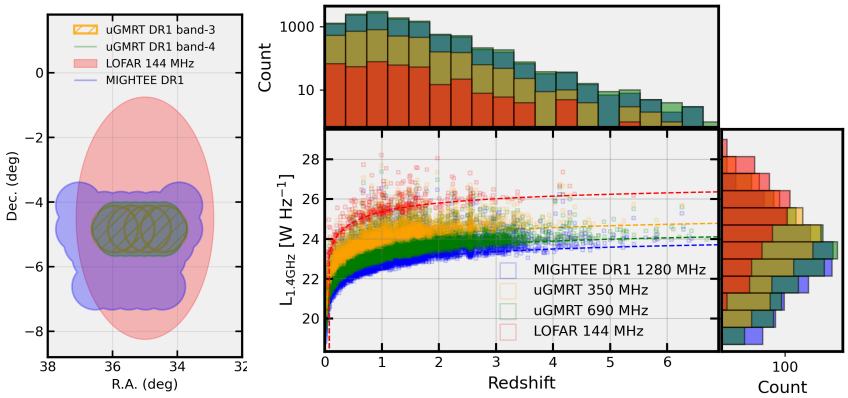

Figure 1: (*Left:*) The survey coverage of the uGMRT band-3 and -4, MIGHTEE DR1, and LOFAR 144 MHz surveys. The area covered is 6.9, 9.9, 14.4 and 27.0 deg^2 respectively. (*Right:*) The 1.4 GHz radio luminosity of the radio continuum surveys mentioned as a function of redshift is provided.

3 Data Analysis

3.1 *Spectral Index and Curvature*

The spectral index is defined as,

$$\alpha = \frac{d\log S_\nu}{d\log \nu} \tag{2}$$

where S_ν is the flux density and ν is the observed frequency. We calculate spectral indices over four frequency bands: uGMRT band-3 (390 MHz) and band-4 (690 MHz) as well as MIGHTEE L-band (1.28 GHz). This yields α_{650}^{1280}, α_{390}^{650}. We plot both these spectral indices against one another, forming a radio-colour plot that defines spectral shapes in each of its quadrants shown in Figure 2. Statistically the distribution of spectral shapes across of the plane indicates $\sim 2\%$ inverted, 78% steep, $\sim 5\%$ concave and 15% peaked radio sources. Additionally, a trend with radio flux density shows an increase peaked and inverted shapes with source brightness as seen in Figure 2. This trend is observed with radio luminosity as well. The thermal noise levels vary between the observed frequency bands with values of 32.0, 8.3, and 3.4 μ Jy/beam for uGMRT band-3, band-4 and MIGHTEE respectively. Hence, incompleteness between bands is likely to be affecting our distribution of observed radio spectral shapes.

3.2 *Simulating Unbiased Spectral Shapes*

A completeness-correction requires us to predict the distribution and number of radio spectral shapes (or types) that would occur without the flux incompleteness between bands. We make use of a Monte Carlo simulation to determine the unbiased radio spectral index distributions. We begin by generating a mock distribution of uGMRT band-4 (B4) flux densities which forms our seed distribution.

We convert B4 flux densities to band-3 (B3) and MIGHTEE mock flux densities by setting up a Gaussian distribution of spectral indices with a fixed mean of $\mu = -0.65$ and the standard deviation to $\sigma_{\rm rms} = 0.5$ for

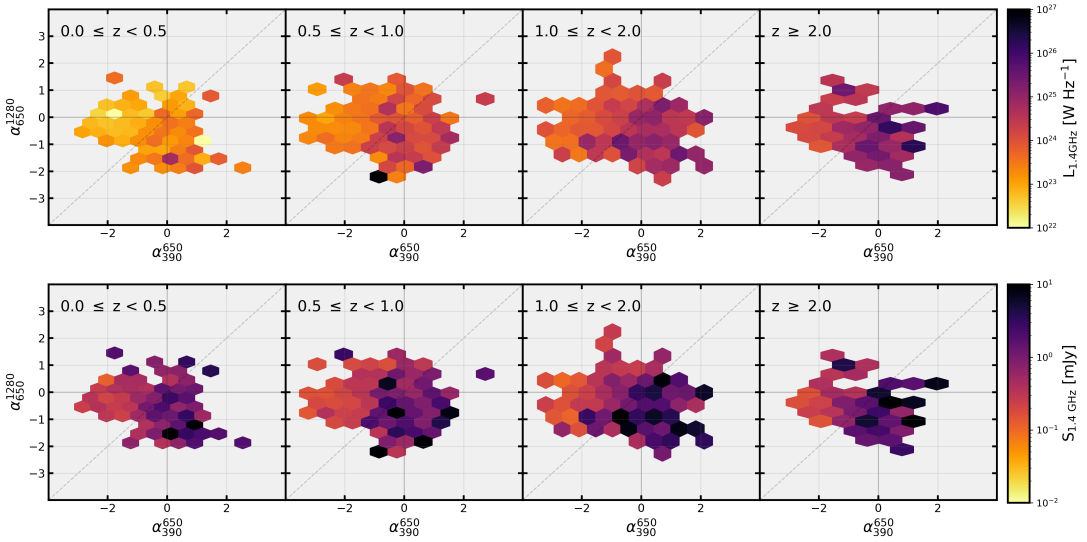

Figure 2: The radio colour-colour plot for superMIGHTEE detected sources across all three frequency bands. The colourbar represents 1.4 GHz flux density and luminosity at the top and bottom, respectively.

the 390-650 MHz distribution and $\mu = -0.45$ and $\sigma = 0.5$ for the 650-1280 MHz distribution based on the observed spectral index distributions. To convert B4 mock fluxes to B3 and MIGHTEE fluxes, we perform random draws of spectral indices from the mock spectral index distributions created. With this method, we generate the underlying flux density distribution for B3 and MIGHTEE DR1. We then inject Gaussian noise to the underlying flux measures such that,

$$f_i = s_i + \delta_i \tag{3}$$

where f_i is the total flux, s_i is the underlying flux and δ_i represents the thermal noise inferred randomly from a distribution centred at $\mu = 0$ with a standard deviation equivalent to the $\sigma_{\rm rms}$ (flux limit) at a given frequency band. We then perform a $\rm S/N = 5$ cut on the mock flux density distributions. We use these mock flux densities to simulate spectral indices in the realistic case where thermal noise values are equivalent to those in the real surveys (for the *Monte Carlo: observed simulation*). We also simulate spectral indices in the ideal case where the thermal noise is identical across all observed frequency bands (for *Monte Carlo: underlying*).

4 Results

We compare the observed spectral indices to the Monte-Carlo simulated ones in Figure 3. The Monte Carlo simulation predicts a higher proportion of flat spectrum sources at flux densities of 300μJy/beam at the low frequency range of 390-650 MHz. For the higher frequency range, a higher proportion of flat spectrum is expected across 650-1280 MHz. Both of these discrepancies between observation and simulation are a result of flux-limit biases in the observations. At low observed frequencies, the faint sources which have flat spectra are missed due to the high uncertainty in thermal noise at lower frequencies (Eddington bias). At higher frequencies, flat spectrum sources are not observed as they are significantly faint in comparison to radio-loud AGN which dominate the population at the redshift limit of the survey (Malmquist bias).

5 Conclusion

Exploiting the heightened sensitivity of the uGMRT and MeerKAT arrays, we have assembled a radio continuum survey dataset for the superMIGHTEE survey covering the XMM-LSS field. We have used four frequency bands, uGMRT band-3, band-4, MIGHTEE DR1. Our observed spectral shapes are dominated by steep spectrum sources which we find to be an artefact of incompleteness between the observed radio frequency bands. Using Monte Carlo simulations, we predict both the underlying distribution of spectral indices for a complete sample. We find a discrepancy between simulation and observation such that faint flat spectrum are missed at low frequencies due to the Eddington bias. Bright flat spectrum sources are missed due to the Malmquist bias which results in a dominance of more powerful radio-loud AGN at the highest redshifts probed by the optical/NIR surveys.

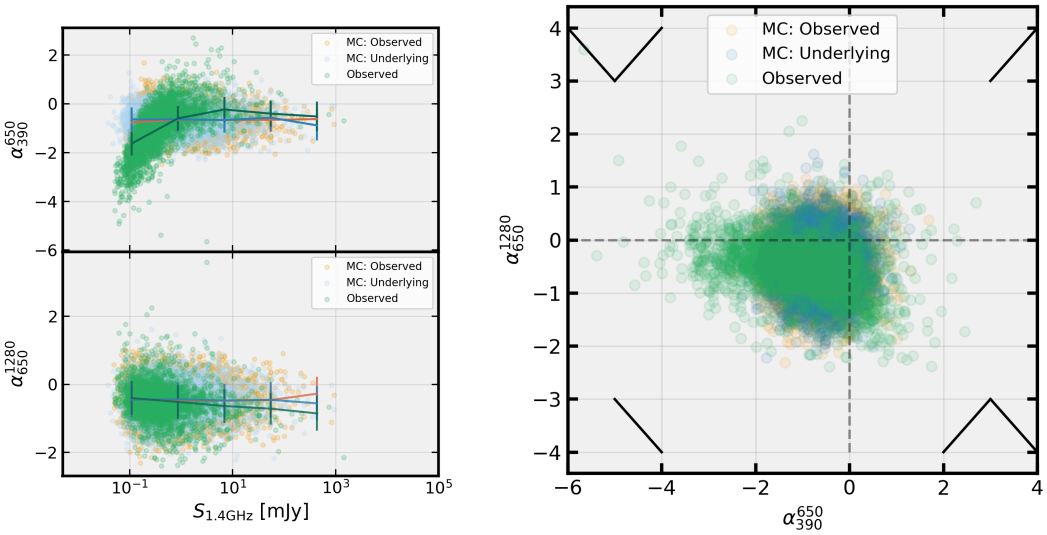

Figure 3: (*Left:*) The observed spectral index as a function of 1.4 GHz flux density shown against Monte Carlo simulated observed (*MC: Observed*) and underlying (*MC: Underlying*) distributions over frequency ranges, 390-650 MHz (*top*) and 650-1280 MHz (*bottom*). We provide a line joining the flux binned medians where the uncertainties are denoted by standard deviations within each flux bin. The lines for observed, *MC: Observed* and *MC: Underlying* are provided in green, red, and blue respectively. (*Right:*) The observed spectral spectral curvature distribution shown against Monte Carlo simulated observed (*MC: Observed*) and underlying (*MC: Underlying*) distributions over frequency ranges, 390-650 MHz (*top*) and 650-1280 MHz (*bottom*).

References

[1] M. Jarvis, R. Taylor, I. Agudo, J. R. Allison, R. P. Deane, B. Frank, N. Gupta, I. Heywood, N. Maddox, K. McAlpine, M. Santos, A. M. M. Scaife, M. Vaccari, J. T. L. Zwart, E. Adams, D. J. Bacon, A. J. Baker, B. A. Bassett, P. N. Best, R. Beswick, S. Blyth, M. L. Brown, M. Bruggen, M. Cluver, S. Colafrancesco, G. Cotter, C. Cress, R. Davé, C. Ferrari, M. J. Hardcastle, C. L. Hale, I. Harrison, P. W. Hatfield, H. R. Klockner, S. Kolwa, E. Malefahlo, T. Marubini, T. Mauch, K. Moodley, R. Morganti, R. P. Norris, J. A. Peters, I. Prandoni, M. Prescott, S. Oliver, N. Oozeer, H. J. A. Rottgering, N. Seymour, C. Simpson, O. Smirnov, and D. J. B. Smith, "The MeerKAT International GHz Tiered Extragalactic Exploration (MIGHTEE) Survey," in *MeerKAT Science: On the Pathway to the SKA*, Jan. 2016, p. 6.

[2] J. J. Condon, "Radio emission from normal galaxies." *ARA&A*, vol. 30, pp. 575–611, Jan. 1992.

[3] G. de Zotti, M. Massardi, M. Negrello, and J. Wall, "Radio and millimeter continuum surveys and their astrophysical implications," *A&A Rev.*, vol. 18, no. 1-2, pp. 1–65, Feb. 2010.

[4] M. J. Hardcastle and J. H. Croston, "Radio galaxies and feedback from AGN jets," *New A Rev.*, vol. 88, p. 101539, Jun. 2020.

[5] P. N. Best, R. Kondapally, W. L. Williams, R. K. Cochrane, K. J. Duncan, C. L. Hale, P. Haskell, K. Małek, I. McCheyne, D. J. B. Smith, L. Wang, A. Botteon, M. Bonato, M. Bondi, G. Calistro Rivera, F. Gao, G. Gürkan, M. J. Hardcastle, M. J. Jarvis, B. Mingo, H. Miraghaei, L. K. Morabito, D. Nisbet, I. Prandoni, H. J. A. Röttgering, J. Sabater, T. Shimwell, C. Tasse, and R. van Weeren, "The LOFAR Two-metre Sky Survey: Deep Fields data release 1. V. Survey description, source classifications, and host galaxy properties," *MNRAS*, vol. 523, no. 2, pp. 1729–1755, Aug. 2023.

[6] J. S. Dunlop, R. J. McLure, A. D. Biggs, J. E. Geach, M. J. Michałowski, R. J. Ivison, W. Rujopakarn, E. van Kampen, A. Kirkpatrick, A. Pope, D. Scott, A. M. Swinbank, T. A. Targett, I. Aretxaga, J. E. Austermann, P. N. Best, V. A. Bruce, E. L. Chapin, S. Charlot, M. Cirasuolo, K. Coppin, R. S. Ellis, S. L. Finkelstein, C. C. Hayward, D. H. Hughes, E. Ibar, P. Jagannathan, S. Khochfar, M. P. Koprowski, D. Narayanan, K. Nyland,

C. Papovich, J. A. Peacock, G. H. Rieke, B. Robertson, T. Vernstrom, P. P. v. d. Werf, G. W. Wilson, and M. Yun, "A deep ALMA image of the Hubble Ultra Deep Field," *MNRAS*, vol. 466, no. 1, pp. 861–883, Apr. 2017.

[7] P. Padovani, "The faint radio sky: radio astronomy becomes mainstream," *A&A Rev.*, vol. 24, no. 1, p. 13, Sep. 2016.

[8] C. Gruppioni, M. Mignoli, and G. Zamorani, "Optical identifications and spectroscopy of a faint radio source sample: the nature of the sub-mJy population," *MNRAS*, vol. 304, no. 1, pp. 199–217, Mar. 1999.

[9] M. Magliocchetti, S. J. Maddox, J. V. Wall, C. R. Benn, and G. Cotter, "The redshift distribution of FIRST radio sources at 1mJy," *MNRAS*, vol. 318, no. 4, pp. 1047–1067, Nov. 2000.

[10] I. Prandoni, L. Gregorini, P. Parma, H. R. de Ruiter, G. Vettolani, A. Zanichelli, M. H. Wieringa, and R. D. Ekers, "The ATESP radio survey. IV. Optical identifications and spectroscopy in the EIS-A region," *A&A*, vol. 369, pp. 787–796, Apr. 2001.

[11] T. M. Heckman and P. N. Best, "The Coevolution of Galaxies and Supermassive Black Holes: Insights from Surveys of the Contemporary Universe," *ARA&A*, vol. 52, pp. 589–660, Aug. 2014.

[12] P. A. G. Scheuer and P. J. S. Williams, "Radio Spectra," *ARA&A*, vol. 6, p. 321, Jan. 1968.

[13] C. L. Carilli, R. A. Perley, J. W. Dreher, and J. P. Leahy, "Multifrequency Radio Observations of Cygnus A: Spectral Aging in Powerful Radio Galaxies," *ApJ*, vol. 383, p. 554, Dec. 1991.

[14] C. L. Hale, I. Heywood, M. J. Jarvis, I. H. Whittam, P. N. Best, F. An, R. A. A. Bowler, I. Harrison, A. Matthews, D. J. B. Smith, A. R. Taylor, and M. Vaccari, "MIGHTEE: the continuum survey Data Release 1," *MNRAS*, vol. 536, no. 3, pp. 2187–2211, Jan. 2025.

[15] M. J. Jarvis, D. G. Bonfield, V. A. Bruce, J. E. Geach, K. McAlpine, R. J. McLure, E. González-Solares, M. Irwin, J. Lewis, A. K. Yoldas, S. Andreon, N. J. G. Cross, J. P. Emerson, G. Dalton, J. S. Dunlop, S. T. Hodgkin, F. O. Le, M. Karouzos, K. Meisenheimer, S. Oliver, S. Rawlings, C. Simpson, I. Smail, D. J. B. Smith, M. Sullivan, W. Sutherland, S. V. White, and J. T. L. Zwart, "The VISTA Deep Extragalactic Observations (VIDEO) survey," *MNRAS*, vol. 428, no. 2, pp. 1281–1295, Jan. 2013.

[16] H. Aihara, R. Armstrong, S. Bickerton, J. Bosch, J. Coupon, H. Furusawa, Y. Hayashi, H. Ikeda, Y. Kamata, H. Karoji, S. Kawanomoto, M. Koike, Y. Komiyama, D. Lang, R. H. Lupton, S. Mineo, H. Miyatake, S. Miyazaki, T. Morokuma, Y. Obuchi, Y. Oishi, Y. Okura, P. A. Price, T. Takata, M. M. Tanaka, M. Tanaka, Y. Tanaka, T. Uchida, F. Uraguchi, Y. Utsumi, S.-Y. Wang, Y. Yamada, H. Yamanoi, N. Yasuda, N. Arimoto, M. Chiba, F. Finet, H. Fujimori, S. Fujimoto, J. Furusawa, T. Goto, A. Goulding, J. E. Gunn, Y. Harikane, T. Hattori, M. Hayashi, K. G. Hełminiak, R. Higuchi, C. Hikage, P. T. P. Ho, B.-C. Hsieh, K. Huang, S. Huang, M. Imanishi, I. Iwata, A. T. Jaelani, H.-Y. Jian, N. Kashikawa, N. Katayama, T. Kojima, A. Konno, S. Koshida, H. Kusakabe, A. Leauthaud, C.-H. Lee, L. Lin, Y.-T. Lin, R. Mandelbaum, Y. Matsuoka, E. Medezinski, S. Miyama, R. Momose, A. More, S. More, S. Mukae, R. Murata, H. Murayama, T. Nagao, F. Nakata, M. Niida, H. Niikura, A. J. Nishizawa, M. Oguri, N. Okabe, Y. Ono, M. Onodera, M. Onoue, M. Ouchi, T.-S. Pyo, T. Shibuya, K. Shimasaku, M. Simet, J. Speagle, D. N. Spergel, M. A. Strauss, Y. Sugahara, N. Sugiyama, Y. Suto, N. Suzuki, P. J. Tait, M. Takada, T. Terai, Y. Toba, E. L. Turner, H. Uchiyama, K. Umetsu, Y. Urata, T. Usuda, S. Yeh, and S. Yuma, "First data release of the Hyper Suprime-Cam Subaru Strategic Program," *PASJ*, vol. 70, p. S8, Jan. 2018.

[17] S. Arnouts and O. Ilbert, "LePHARE: Photometric Analysis for Redshift Estimate," Astrophysics Source Code Library, record ascl:1108.009, Aug. 2011.

[18] P. W. Hatfield, M. J. Jarvis, N. Adams, R. A. A. Bowler, B. Häußler, and K. J. Duncan, "Hybrid photometric redshifts for sources in the COSMOS and XMM-LSS fields," *MNRAS*, vol. 513, no. 3, pp. 3719–3733, Jul. 2022.

[19] K. J. Duncan, M. J. Jarvis, M. J. I. Brown, and H. J. A. Röttgering, "Photometric redshifts for the next generation of deep radio continuum surveys - II. Gaussian processes and hybrid estimates," *MNRAS*, vol. 477, no. 4, pp. 5177–5190, Jul. 2018.

[20] N. Mohan and D. Rafferty, "PyBDSF: Python Blob Detection and Source Finder," p. ascl:1502.007, Feb. 2015.